Fluorine- and Niobium-Doped TiO2: Chemical and Spectroscopic Properties of Polycrystalline n-Type-Doped Anatase

Jakub Biedrzycki,Stefano Livraghi,Elio Giamello,Stefano Agnoli,Gaetano Granozzi

Fluorine- and Niobium-Doped TiO2: Chemical and Spectroscopic Properties of Polycrystalline n-Type-Doped Anatase

JOURNAL OF PHYSICAL CHEMISTRY. C, NANOMATERIALS AND INTERFACES (2014) 118
DOI: 10.1021/jp501203h

Fluorine and Niobium doped TiO_2: chemical and spectroscopic properties of polycrystalline n-type doped anatase.

Jakub Biedrzycki[a], Stefano Livraghi[a], Elio Giamello[a]*, Stefano Agnoli[b], Gaetano Granozzi[b]

Dipartimento di Chimica, Università di Torino, Via P. Giuria 7, 10125 Torino (IT)

Dipartimento di Scienze Chimiche, Università di Padova, Via Marzolo 1, 35131 Padova (IT)

Abstract

Doping titanium dioxide (anatase) with elements carrying an extra electron such as Nb and F or with mixtures of both elements, leads to n-type materials showing peculiar properties with respect to the pristine oxide. Niobium and fluorine are present in the lattice under the form of Nb^{5+} and F^- ions (detected by XPS) and the extra electrons carried by the dopants are stabilized on titanium ions which become EPR visible as Ti^{3+} ions homogeneously dispersed in the bulk of the crystals. In such conditions the band gap optical transition is slightly red shifted (few tenths of eV) for all samples containing fluorine and the Fermi level lies, according to the materials, at the boundary or even in the lower region of the conduction band. The typical Ti^{3+}(I) centers generated by valence induction are responsible of the already reported conductivity properties of the system. The presence of these centers also influence the process of electron injection in the solid favoring the dilution of additional reduced centers in the bulk, leading to a homogeneously reduced material with optoelectronic properties differing from those of reduced anatase.

Keywords: n-type doped TiO_2, Ti^{3+}, EPR, DR-UV-Vis, conductivity, Fermi level.

1. Introduction.

Titanium dioxide is one of the most investigated metal oxides. The importance of this abundant, cheap and non toxic material is certainly due its large scale applications as a white pigment. However the great deal of scientific investigations concerning this oxide is essentially due to the exciting applications related to its photochemical and photophysical properties. This explains the exponential growth of papers devoted to both bare and modified TiO_2 appeared in the literature in the past twenty years[1,2]. Titanium dioxide (or titania) is the most important photocatalyst, active in several reactions for pollutants abatement[3] and, since the discovery of water photosplitting in 1972[4], it can also be considered as a system of interest for photochemical and photo-electrochemical applications in energetics (artificial photosynthesis). Furthermore titanium dioxide is employed as biocide[5], in odour control[6], in the preparation of self-cleaning surfaces and of superhydrophilic antifogging layers[7]. Extremely important is also the use of titanium dioxide in photovoltaics. In dye-sensitized solar cells (DSSC)[8], in fact, it plays the role of acceptor of electrons from the dye excited state and that of electron carrier towards the electric contact.

The main polymorphs of titanium dioxide are rutile and anatase. The former phase is more stable than the latter one, which however, is more effective in terms of photochemical applications. In parallel with the growth of titanium dioxide applications an intense activity begun, devoted to prepare modified forms of the solid in order to tune some of its specific physical properties. This is the case of the inclusion of either transition metal or non-metal impurities into the lattice in order to modify the optical absorption of the system.One of the goals of this activity, even though not the unique one, is to reduce the optical absorption threshold of the oxide, whose band gap is around 3.2 eV for the anatase polymorph (corresponding to a UV photon) and to make it photosensitive to visible light[1,9,10,11].

Among the various types of non-metal doping of TiO_2 that with fluoride ions assumes a particular role. About ten years ago it was reported that the inclusion of fluoride ions into the oxide matrix improves the photocatalytic performance of the bare oxide in the mineralization of various organic pollutants using either UV[12]or visible[13] light. To obtain fluorine doped titania the fluoride ions are usually introduced in the liquid medium for the preparation of the oxide via hydrolysis (for instance by the frequently used sol-gel technique). A fraction of the F^- ions is so included in the lattice where they substitute oxygen O^{2-} anions. An investigation by some of us, based on Electron Paramagnetic Resonance (EPR)[14],on F doped anataseTiO_2 (hereafter F-TiO_2) prepared via sol-gel, clarified that paramagnetic Ti^{3+}ions are present in the solid. This occurs because at least a fraction of the excess electrons introduced by fluorine are localized by lattice Ti^{4+}cations. The presence of reduced Ti^{3+}

centres in the as prepared, fully oxidized solid indicates that the F-TiO_2 system can be described in terms of an n-type semiconductor. It is worth noting that pristine titanium dioxide (belonging to the class of reducible oxides since it easily loses oxygen) also becomes an n-type system when annealed under vacuum, due to oxygen depletion, formation of anion vacancies and excess electrons stabilisation (Ti^{3+}). Fully oxidized, undefective TiO_2 and F-TiO_2 thus differ since the latter only is, intrinsically, an n-type semiconducting system as indicated by early investigations pointing to the electronic and photoelectric properties of F doped rutile TiO_2[15,16].

The same electronic effect described for F-TiO_2 is observed when the tetravalent Ti of anatase is substituted by a pentavalent element such as Nb or Sb. Also in these two cases the extra-electron brought about by the dopant is expected [17] to localise on titanium ions producing Ti^{3+}. The formation of lattice trivalent titanium ions was directly monitored by EPR for Nb-TiO_2 (anatase) in the past[18,19,20]. The interest in Nb doped titania has recently increased due to the search for new transparent conducting oxides (TCO) to employ in optoelectronic devices[21,22,23] and, in particular, in DSSC to promote the charge transport within the transparent oxide layer usually constituted by bare TiO_2[24,25,26]. It is worth mentioning, by the way, that in the case of Nb-TiO_2 the described valence induction effect (i.e. formation of Nb^{5+} and Ti^{3+}) holds for the anatase polymorph, while in the case of rutile doped with niobium the extra-electron remains on the dopant atom as indicated by the presence of Nb^{4+} ions which were detected both by EPR at low temperature for Nb-TiO_2 rutile single crystals[27,28] and by XPS measurements[29].

In the present paper we report a detailed study of the chemical and spectroscopic properties of n-type doped polycrystalline anatase performed with the joint use of optical spectroscopy (DR UV-Vis-NIR), photoelectron spectroscopies and Electron Paramagnetic Resonance (EPR). The materials under investigation were both singly doped systems (F-TiO_2 and Nb-TiO_2) and co-doped (F,Nb) ones. Our investigation started with two main goals. The first one was to explore band gap modifications of TiO_2 depending on the type of dopant. The second goal was that of examining the behaviour of the doped materials upon addition of further electron excess (via direct injections or via reduction) in comparison with the behaviour of pristine TiO_2. The presence and the mobility of excess electrons are essential in photochemical applications of the solid such as photocatalysis or dye sensitized solar cells. A similar approach induced Wold and coworkers[15], more than thirty years ago, to investigate the photoconduction of fluorinated rutile crystals that showed significantly higher conductivity than reduced rutile. More recently, studies on Nb doped anatase have shown similar conductivity increments[24,25].

2. Experimental.

2.1. Samples preparation.

The TiO_2 sample was prepared via sol-gel process using Ti-isopropoxide as Ti precursor as reported in previous work[20]. Doped samples were prepared as described in the following.

2.1.1. F-TiO_2.

This set of samples was prepared via sol-gel using as hydrolyzing agent hydrofluoric acid solutions. In a typical preparation 7.5ml of Ti-isopropoxide was diluted in 7.5ml of 2-propanol and the obtained mixture was hydrolyzed with 4ml of HF solution of different concentration in order to obtain a nominal ratio F/Ti = 0.01, 0.90, 1.80, 3.50, 5.50 and 7.00. The formed solid was dried at 340K and finally calcined at 770K (heating rate 10 K/min) for 1 hour in order to obtain a fully oxidized material and to get rid of all contaminants left from the synthesis. Higher temperatures were not adopted in order to limit fluorine loss[30]. The samples were labelled as F1, F2, F3, F4, F5, and F6 respectively. For sake of brevity, only data related to F2 will be reported in the text. The data related to remaining samples are shown as Supporting Information.

2.1.2. Nb-TiO_2.

This sample was prepared via sol-gel process. An appropriate amount of $NbCl_5$, in order to obtain a nominal doping of 5% (Nb/Ti=0.05) was added to 7.5ml of 2-propanol followed by stirring at room temperature until a complete $NbCl_5$ dissolution. Successively 7.5ml of Ti-isopropoxide was added to the previous mixture. The final solution was hydrolyzed with 4ml of H_2O. The obtained solid was dried at 340K and finally calcined at 770K (heating rate 10K/min) for 1 hour in order to obtain a fully oxidized material and to get rid of all contaminants left from the synthesis. Higher temperature was not adopted in order to avoid anatase to rutile phase conversion. The sample was labelled as Nb1.

2.1.3. F-Nb-TiO_2(co-doped samples).

This set of samples was prepared as follows. The solution containing the cations (Nb, Ti) was prepared as in the previous case and was then hydrolyzed with solutions of hydrofluoric acid having different concentration in order to obtain nominal F/Ti ratios of 0.05, 0.15, 0.25, 0.35 and 0.45. The obtained solids were dried at 340K and finally calcined at 970K (heating rate 10K/min) for 1 hour. In this case, the higher calcination temperature was adopted since fluorine (although partially expelled from the solid in these conditions) stabilizes the anatase phase reducing the conversion to rutile and allows obtaining materials having high crystallinity.

The samples were labelled NbF05, NbF15,NbF25, NbF35 and NbF45 (Table 1).A further sample labelled NbF25a was prepared using H_2O as hydrolyzing agent and NbF_5 as source of both Nb and F. For sake of brevity only data related to samples from NbF25 to NbF45 and sample NbF25a will be reported in the text. The data related to the remaining samples are shown as Supporting Information.

Table 1 resumes the main features and abbreviations for the samples reported in this work. Due to the loss of fluorine which progressively occurs also during the various reductive treatments, the evaluation by chemical analysis of the initial F/Ti ratio is substantially non-significant and therefore has not been performed.

Sample abbreviation	Nb/Ti Nominal	Nb/Ti (XRF)	F/Ti Nominal	Calcination Temp./ K	Phase (w/w %)*			Crystal size*† (nm)	Band gap (Eg)/ eV
					A	R	B		
TiO_2	0	0	0	770	100	0	0	30	3.20
F2	0	---	0.90	770	100	0	0	30	3.20
Nb1	0.05	0.05	0	770	55	10	35	12	2.91
NbF25	0.05	0.05	0.25	970	98	2	0	21	3.03
NbF35	0.05	0.05	0.35	970	100	0	0	24	3.08
NbF45	0.05	0.06	0.45	970	100	0	0	32	3.11
NbF25a	0.05	0.05	0.25	970	100	0	0	23	3.18

Table 1. Abbreviations adopted for the samples of the present work and the corresponding compositional, structural and optical properties: A=Anatase, R=Rutile, B=Brookite.
*Data obtained via Rietveld refinement using the Maud program. † Data related to the anatase polymorph only.

2.2. Structural and spectroscopic characterization of the materials.

XRD patterns were collected on a diffractometer (PW1830, Phillips) using Co (Kα) radiation. Diffraction peaks have been indexed according to the ICSD (Inorganic Crystal Structure Database). The crystallites size of the various investigated materials was obtained by employing the Debye–Scherrer equation. Phase composition was determined via refining the obtained data with Rietveld method using MAUD program[31].

Photoemission data were acquired in a custom designed ultrahigh vacuum (UHV) system equipped with a VG MK II Escalab electron analyser, working at a base pressure of 10^{-10} mbar. Core level photoemission spectra were taken at room temperature in normal emission using a non monochromatized Al/Mg twin anode X-ray source, whereas for valence band data we used a He

discharge lamp (Omicron HIS 15). Powder samples were suspended in bi-distilled water and drop casted on high purity copper foils. After drying in air, the obtained films were introduced in the ultrahigh vacuum system, outgassed overnight, and finally annealed in UHV for 20 minutes at 650 K. The charging observed during measurements of some samples was corrected using the adventitious carbon as internal reference. The energy calibration has been determined by using a gold sample (Au 4f at 84 eV)

The elemental analysis was performed by means of X-ray fluorescence (XRF) spectroscopy. The samples were analyzed using an EDAX Eagle III energy-dispersive micro-XRF(μXRF) spectrometer equipped with a Rh X-ray tube and a polycapillary with a circular area of nominally 30 μm diameter. Data collection occurred at each point for 250 s detector live time, with X-ray tube settings adjusted for 30% dead time.

Diffuse Reflectance Spectroscopy (DR UV-Vis-NIR) was employed to characterize the absorption features in a range of wavelength between UV and NIR (250 – 2500 nm). DR UV-vis measurements were performed on fine powders of the samples in a cell with optical quartz walls. The spectra were collected in the reflectance mode with a Perkin-Elmer Cary5000 instrument equipped with an integrating sphere and then reported as an absorbance-like pattern by means of the Kubelka-Munk function. Optical band gap absorption was obtained by means of aTauc plot of the Kubelka-Munk absorption as a function of the photon energy.

Electron Paramagnetic Resonance (EPR) spectra were run using a X-band CW-EPR Bruker EMX spectrometer equipped with a cylindrical cavity operating at 100 kHz field modulation. The measurements were carried out at 77 K in cells that can be connected to a conventional high-vacuum apparatus (residual pressure $<10^{-4}$mbar).

3. Results and Discussion.

3.1. Composition and structural features of fluorine and niobium doped titanium dioxide.

In the present paper we report results concerning two singly doped titania samples (with F and Nb) and four co-doped materials. A sample of bare anatase (TiO_2) prepared with the same procedure (Section 2) was used for comparison. Results on a wider collection of doped and co-doped samples are available as Supporting Information (S.I.). Table 1 presents some basic features of the samples here examined. The atomic ratios between the anionic dopant (F^-) and titanium are relative to the composition of the liquid phase prior gelification and do not represent the actual composition of the solid [14,30], because it is known that a fraction of fluorine is eliminated from the solid during the

final calcination of the materials. The four co-doped solids were prepared using a constant Nb concentration (Nb/Ti = 0.05) and varying that of fluorine. As far as the cationic dopant is concerned the μXRF analysis has shown a good correspondence between the nominal and the final Nb/Ti content for all Nb containing samples (see Table 1).

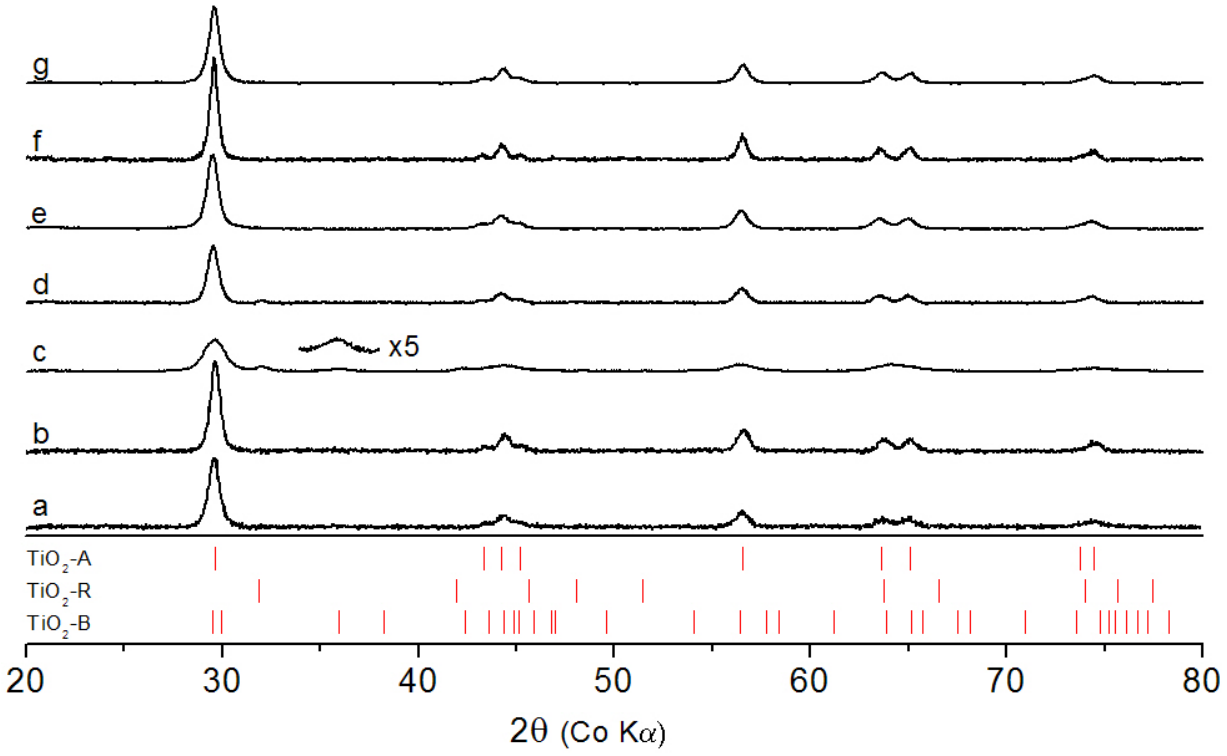

Figure 1.XRD patterns of TiO_2 based materials: a) TiO_2, b) F2, c) Nb1, d) NbF25, e) NbF35, f) NbF45, g) NbF25a. The sticks corresponding to TiO_2-A, TiO_2-R, and TiO_2-B indicate the diffraction peaks of the anatase, rutile and brookite polymorphs respectively.

Fig.1 shows the XRD plot of all samples described in Table 1. Anatase is the unique phase in all samples except for Nb1 (Nb-TiO_2, Fig. 1c) that shows the presence of rutile and brookite and for the low fluorine content NbF25 that exhibits traces of rutile (Fig. 1d). It is known, in fact, that the presence of fluorine allows the formation of a highly crystalline anatase phase. This state is achieved because F, inhibiting the anatase to rutile transition, allows one to reach relatively high temperatures of calcination. At these temperatures a better quality of the anatase crystals is obtained. This latter factor has been invoked as the reason of the good photocatalytic performances of fluorine doped anatase powders [30]. The solubility of fluorine in TiO_2 is however limited by two factors. The first one is the mentioned elimination of this element during calcination; the second one

is the formation of an extra phase amenable to $TiOF_2$ occurring for high fluorine concentrations[13] (see S.I., Fig. SI1).

The behaviour of niobium is different from that of fluorine since Nb ions can be incorporated in TiO_2 in a wider range of concentrations[32]. The presence of niobium, however, does not completely suppress the formation of rutile even at relatively low calcination temperatures. The Nb-TiO_2 sample (Nb1, Table 1 and Fig 1 c) in fact contains about 10% w/w of rutile after calcination at 773 K.

To obtain single phase (anatase) materials the drawbacks of the two single doping procedures can be overcome using co-doping with the two elements. Niobium is not removed at high temperature ensuring a certain degree of n-doping, while the presence of fluorine stabilizes the anatase polymorph.

3.2. Optical properties of (oxidized) n-type doped TiO_2.

The optical properties of the various doped and co-doped TiO_2 samples are illustrated in Fig. 2 by DR UV-Vis spectra. All the spectra are dominated by a strong absorption in the UV region due to the transition from the valence band to the conduction band whose absorption threshold, however, changes in the case of doped systems.

Except for NbF25a, which is prepared by a different procedure and shows an absorption edge basically coincident with that observed for pure TiO_2, all samples show a red-shift of few tenth of eV with respect to the absorption threshold of bare TiO_2. The Nb-TiO_2 (Nb1) sample exhibits the larger red shift and the material shows a yellowish colour (Fig. 2, black line). This sample is however the only one containing appreciable amounts of the other two TiO_2 polymorphs (Table 1) namely brookite (with band gap similar to that of anatase[33]) and rutile, which has a smaller band gap than anatase. In the majority of cases of Nb doped titania reported in the literature, however, blue shift of the band gap edge is observed, which is explained in terms of the Burstein-Moss effect [18,24,25,34,35,36]. This effect is based on the conduction band filling by extra electrons that suppresses absorption at the band edge. Nevertheless in some other cases a red shift, like in the present work, has been reported for Nb-TiO_2[37,38,39,40,41]. There are also examples in which no change in the optical spectra is observed[42,43]. An unambiguous interpretation of the red-shift is not present in the literature. Some Authors explain this experimental evidence invoking the presence of Nb_2O_5 micro-aggregates in the TiO_2 matrix[38]. Even though there is no trace of niobium oxides in XRD diffractions of our samples (Fig.1) (which could be due to quantitative limits of the technique or to the presence of amorphous fractions) the fact remains that the Burstein-Moss effect does not occur

in Nb doped and Nb-F co-doped materials prepared via sol-gel for which a red-shift of the absorption edge is systematically observed.

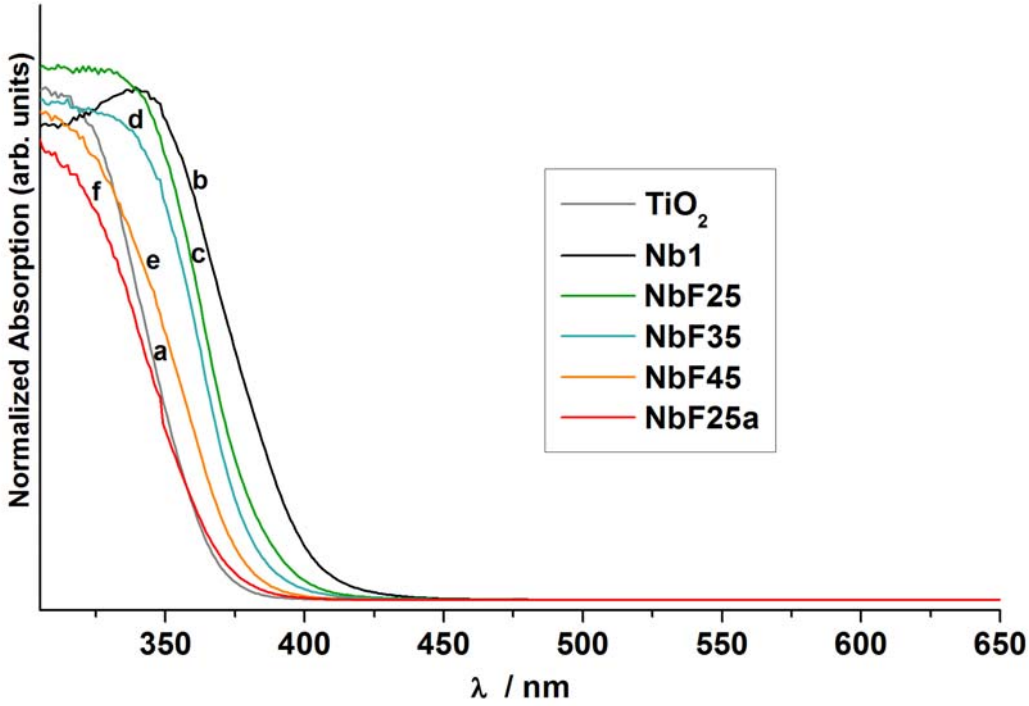

Figure 2. DR UV-Vis spectra: a) TiO_2, b) Nb1, c) NbF25, d) NbF35, e) NbF45, f) NbF25a.

In the spectroscopic region between 450 and 650 nm the spectral lines are flat for all samples and there is no evidence of absorption in the visible. The same occurs in the IR region till 2500 nm (*vide infra*). This result differs from what reported in some case of Nb doped titania, like for instance in the recent paper by De Trizio *et al.*[26] who obtained blue colored materials. This considerable difference is very probably due to the partial reduced state of their colloidal samples (see Section 3.6 on the optical properties of reduced materials). A similar situation is described by Sauvage, Graetzel and collaborators[25] who prepared Nb-TiO_2 suspensions by hydrothermal reaction also obtaining blue materials that, however, after treatment at 770 K or long air exposure definitely turn to white. In the case of the materials described in the present paper (having a relatively low Nb loading) in spite of the presence of Ti^{3+} reduced centres revealed by EPR no optical absorption in the visible occurs and the samples, except for the pale yellow Nb1 (whose color is due to the band gap transition tail), are white.

3.3. EPR of doped and co-doped materials.

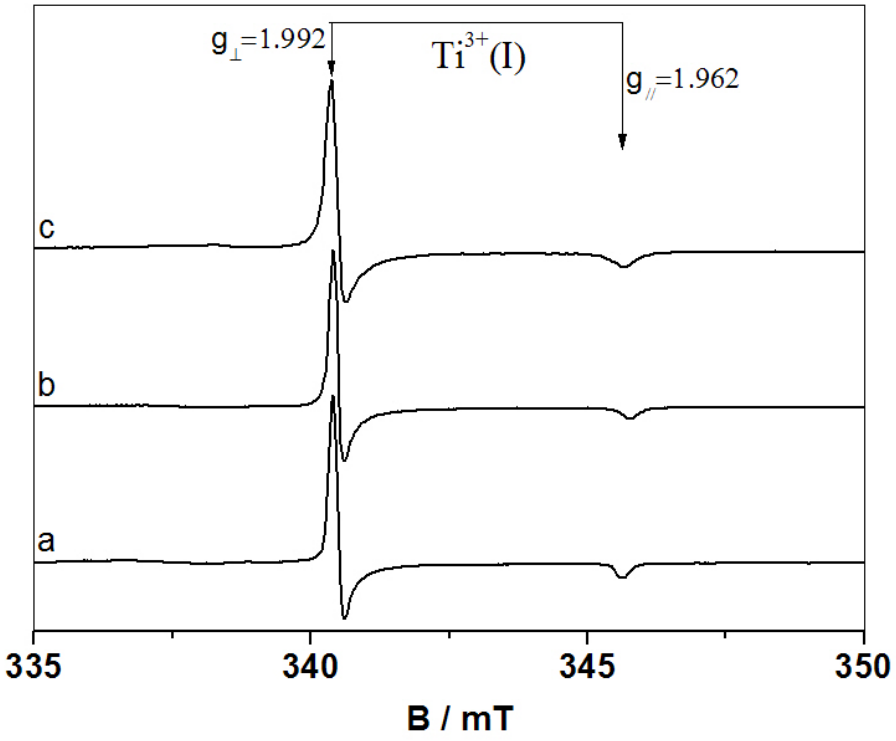

Figure 3. Normalized EPR spectra recorded at 77K of n-type TiO_2: a)F2, b)Nb1and c) NbF45.

As recalled in the introduction the alio-valent substitution (F or Nb) implies the presence of excess electrons in the system that leads to the formation of Ti^{3+}centres by a mechanism of valence induction. These ions are paramagnetic and the corresponding EPR spectra recorded at 77K (Fig. 3) have been conclusively assigned in our previous work to reduced Ti^{3+} centres in regular lattice sites in the bulk of the anatase matrix[44]. For both dopants the signal is axial and characterized by $g_{\perp}$=1.992, $g_{//}$=1.962. The same signal (hereafter Ti^{3+}(I))is observed in the case of co-doped materials (Fig. 3). It is worth recalling that the samples whose spectra are reported in Fig. 3 are fully oxidized materials (See Experimental) and that the presence of Ti^{3+} ions is uniquely due to the valence induction effect and not to a partial reduction of the solid (*vide infra*). These reduced titanium ion are well dispersed in the solid matrix (relatively narrow linewidth) and there is no evidence of appreciable amounts of surface reduced ions, which have different EPR parameters[20].

Summarizing, both F-TiO_2 and Nb-TiO_2 can be described as n-type doped oxides (electrically neutral systems containing, with respect to the bare oxide, extra electrons conveyed by the presence of diluted aliovalent elements). Their formulas, which can be written, as a first approximation and

on the basis of the valence induction effect, as $Ti^{4+}_{(1-x)}Ti^{3+}_{x}\ F^{-}_{x}\ O^{2-}_{(2-x)}$ and $Ti^{4+}_{(1-2x)}Nb^{5+}_{x}Ti^{3+}_{x}O^{2-}_{2}$ respectively, point to the stabilisation of the extra electrons on lattice titanium ions as indicated by the EPR spectra which are the same in both cases. The co-doped systems can be described by a combination of the two previous formulas. Another compensation mechanism based on the formation of Ti^{4+} vacancies, which has been proposed based on conductivity measurements[24], cannot in principle be excluded and will be discussed in Section 4. The features of the EPR spectra, however, unambiguously indicate that at least a fraction of the dopant (F or Nb) releases excess electrons into the solid producing donor Ti^{3+} centres that modify therefore the electronic structure of the solid itself.

3.4. XPS Characterization.

In order to investigate the compositional features and the electronic structure of the doped solids a detailed investigation based on photoelectron spectroscopy was carried out. In figure 4 we report the core level spectra of Ti 2*p* and Nb 3*d* : in all samples the Ti $2p_{3/2}$ peak maximum is centered at 459 eV, it is highly symmetric and, despite the EPR evidence reported above, does not show any significant presence of the shoulder connected to Ti^{3+} reduced species at 457.5 eV. Similarly, the Nb 3*d* photoemission line shows a highly symmetric doublet with the maximum centered at 207.5 eV, which nicely corresponds to Nb^{5+} species[26,45]. This dopant is therefore present into the systems in its maximum oxidation state. A small shift at slightly lower binding energy is observed for the sample Nb1 only. Fluoride dopants are observed in relatively small concentrations and no other impurities except for C (< 0.5%) were detected. A quantitative analysis of the surface and subsurface region accessible to X-rays has been performed using two sources (Mg and Al) having different penetration (Table 2). The intensity of the photoemission spectra has been normalized using the differential cross sections and asymmetry parameters provided by Yeh and Lindau[46] and the inelastic mean free path calculated using the TPP2 algorithm[47]. Table 2 indicates that the Nb concentrations found in the various samples are quite similar, the Nb/Ti ratio being around 0.2 with the only exception of Nb1, where this value is around 0.11. These values, however, are definitely higher than both the nominal compositions and the XRF values (Table 1).

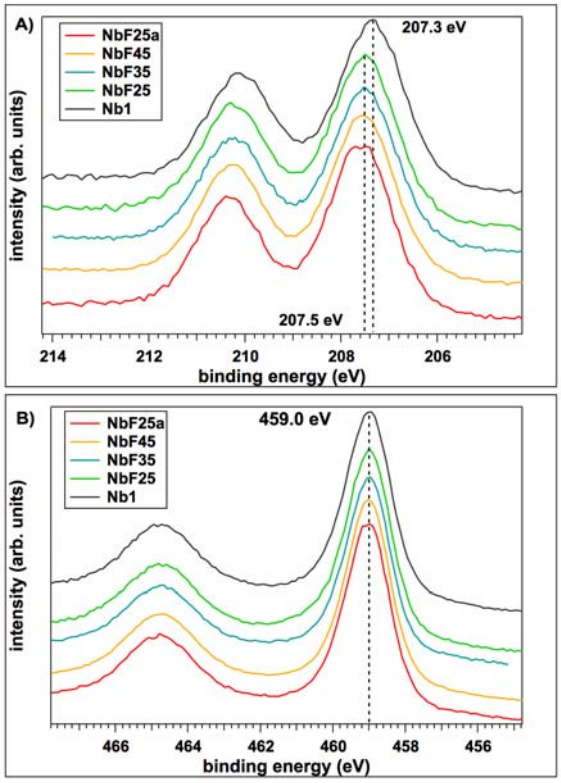

Figure 4. XPS core level spectra of A) Nb 3*d* and B) Ti 2*p*; a) Nb1, b) NbF25, c) NbF35, d) NbF45, e) NbF25a.

This difference is due to the fact that XPS, a surface technique, monitors a limited subsurface region so that one can gather that the niobium distribution is not homogeneous and that a gradient of concentration exists moving from the surface to the center of the nanocrystals. This fact is confirmed by comparing the compositional data obtained with the two sources. Nb concentrations, in fact, are systematically higher in the case of the Mg source (l253.6 eV)than in that of the Al one (1486.6eV), which probes deeper layers due to a higher energy of photo-electrons. The gradient of niobium concentration seems an unavoidable feature of our preparation method but should not influence the general behavior of the solids. For this reason it will not be further discussed. XPS data also indicate an excess of oxygen probably due the presence of surface hydroxyl groups and/or chemisorbed water that alters the solid stoichiometry at the surface. Residual concentrations of fluoride ions, ranging from 1% to 9%, are detected in all samples. Even though the real concentration of F in the whole sample is unknown, these XPS results corroborate the idea that a fraction of fluorine leaves the solid during the final thermal treatment. Nonetheless, the presence of both Nb and residual fluoride ions indicates that the prepared materials can be considered as n-type co-doped anatase systems with the only exception of Nb1, which is doped with Nb only and contains fractions of other polymorphs.

Sample	Mg Kα (1253,6 eV)	Al Kα (1486.6 eV)	VBM (eV)	E_F = Eg-VBM (eV)
NbF25a	$Ti_1O_{2.72}Nb_{0.18}F_{0.09}$	$Ti_1O_{2.82}Nb_{0.15}F_{0.03}$	3.20	-0.02
NbF45	$Ti_1O_{2.79}Nb_{0.2}1F_{0.055}$	$Ti_1O_{2.83}Nb_{0.17}F_{0.05}$	3.15	-0.04
NbF35	$Ti_1O_{2.89}Nb_{0.2}F_{0.05}$	$Ti_1O_{2.94}Nb_{0.15}F_{0.012}$	3.25	-0.17
NbF25	$Ti_1O_{2.81}Nb_{0.19}F_{0.01}$	$Ti_1O_{2.85}Nb_{0.13}F_{0.03}$	3.20	-0.17
Nb1	$Ti_1O_{2.44}Nb_{0.11}F_{0.0}$	$Ti_1O_{2.5}Nb_{0.11}F_{0.0}$	2.80	0.11

Table 2. Column 2 and 3: Compositional values of the various materials derived using a Mg and an Al source respectively; Column 4: Valence Band Maximum (VBM); Column 5: Fermi energy levels (E_F) estimated combining VBM values with the optical band gap values (Eg).

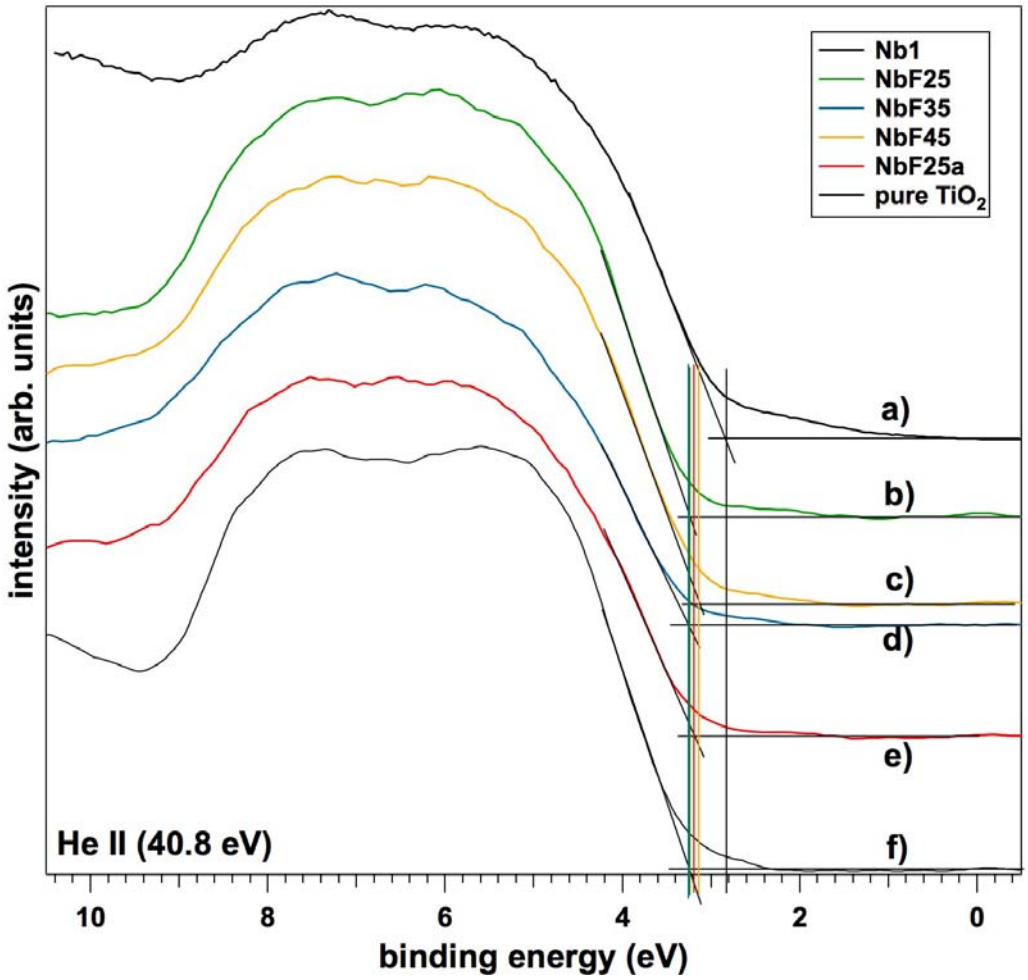

Figure 5. Valence Band spectra: a) Nb1, b) NbF25, c) NbF35, d) NbF45, e) NbF25a, f) TiO_2.

A further insight into the electronic properties of the materials can be provided by Ultraviolet Photoemission Spectroscopy (UPS). In figure 5 we report the valence band spectra acquired using the He II emission line (hν=40.8 eV). The spectra indicate the presence of a semiconductive gap with minimal differences with respect to pure TiO_2. The typical defect band at a binding energy of 1 eV due to Ti^{3+} species, which is generally found in the case of reduced TiO_2, is not detected. By applying a widely used procedure for titania based materials, we have interpolated by a line the low energy slope of the valence band and used its intercept with the energy axis for a qualitative determination of the valence band maximum (VBM) position[48,49,50]. The results are quite similar for all samples, which are very close to the value of bare anatase ($E_{VB,max}$~3.2 eV)[48], with the notable exception of sample Nb1 whose valence band edge is found at 2.8 eV, a value well in agreement with previous investigation of Nb doped titania by DR UV-Vis Spectroscopy. Combining the VBM values with the estimated optical band gap (Table 1), it is possible to deduce the Fermi level energy (E_F) for the whole set of samples[49] (see Table 2). It is worth to note that the Energy gap has been obtained via a method which implicates a certain degree of approximation[51]. The absolute E_F value is obviously quite dependent on the binding energy range used for the linear interpolation of the slope of the valence band[52], however this approach is quite reliable if used, as in the present case, to compare the values in a series of homologous materials. The whole set of data indicate therefore that in our materials, as expected for n-type systems, the Fermi level lies, in an higher position with respect to the undoped material, very close to the conduction band minimum (CBM) as aspected for Nb-doped system[53] ore, in some case, even inside the conduction band in agreement with findings predicting by theoretical approach[54,55].

As to the red shift observed for Nb containing materials leading to some absorbance in the visible region (Fig. 2), combining UPS and DR-UV-Vis data we can infer that this is not ascribable to the presence of localized states like for example in the case of reduced blue titania, but rather to a general broadening of the valence band that is moving towards lower binding energies thus narrowing the band gap.

3.5. Excess electron injection in n-type doped TiO_2.

Formation, stabilisation and migration of charge carriers in TiO_2 are phenomena of paramount importance due to the photochemical (photoinduced charge separation) and optoelectronic applications (transparent conducting materials) of this oxide. Charge dynamics in particular has been investigated in terms of the alternative mechanisms of ohmic and polaronic electronic conduction[56,57] while the nature of localized electron centres has been tackled trying to understand

the space distribution of the trapped electron wave function. This question is still debated and opposite conclusions (electron localized on a single titanium ion or delocalized on several ions in a relatively large volume) have been proposed on the basis of different approaches[58,59]. The recent activity of our group has challenged the problem of localisation vs. delocalisation of excess electrons in both anatase and rutile[20,60] exploring the EPR spectra of the corresponding centres generated either by irradiation or by chemical reactions (electron injection, reduction by annealing and consequent oxygen depletion). We will illustrate in the following a series of experiments performed with the same approach on n-type doped anatase.

3.5.1. Electrons injection.

A simple method to introduce excess electrons in TiO_2 is based on the reactivity of the solid with atomic hydrogen. This can be performed either generating the reactant via microwave discharge in H_2 atmosphere or irradiating the system, always in the presence of H_2, with UV light. In the first case the H atom ionizes injecting an electron into the solid[61,62] ($O^{2-}_{surf} + H \rightarrow OH^{-}_{surf} + e^{-}$). In the second case the UV radiation induces the formation of an electron-hole pair. The hole, once migrated at the surface, reacts with molecular hydrogen to give an hydroxyl group and an H atom that, as in the previous case, ionizes injecting an electron into the solid ($2O^{2-}_{surf} + h^{+} + H_2 \rightarrow OH^{-}_{surf} + O^{2-}_{surf} + H^{\bullet} \rightarrow 2OH^{-}_{surf} + e^{-}$). Excess electrons are successively stabilized on Ti^{4+}cations forming Ti^{3+} centres ($Ti^{4+} + e^{-} \rightarrow Ti^{3+}$).

The result of this latter experiment in the case of bare TiO_2 anatase is reported in Fig. 6 (panel A). The base line (line a) in this case is flat since no paramagnetic species are present in the pristine oxide. Irradiation in the presence of H_2 generates an intense EPR spectrum due to the overlap of two independent signals both amenable to Ti^{3+} species (Ti^{3+}(I) and Ti^{3+}(II)). While the former species is due to electrons stabilized on regular Ti^{4+} sites of the anatase bulk (Ti^{3+}(I) is the same signal shown in Fig. 3 for doped materials), the second species (much more abundant than the previous one because of its large linewidth) is related to trapping sites present at the surface of the system. The large line width of this signal is due to the relatively disordered environment typical of anatase nanocrystals. The surface nature of Ti^{3+}(II) species has been conclusively demonstrated on the basis of Pulse-EPR experiments using ^{17}O[20].

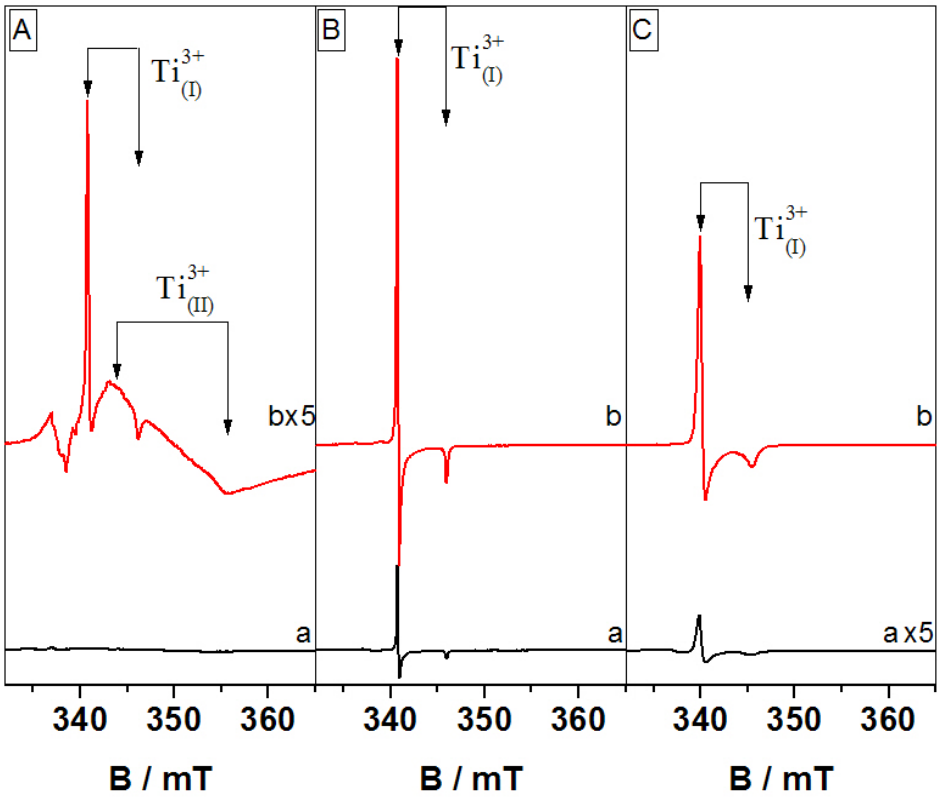

Figure 6. EPR spectra of bare anatase and n-type TiO_2 samples obtained after UV irradiation at 77K in presence of H_2: a) TiO_2, b) NbF45, c) Nb1.

The same irradiation experiment was then performed using two distinct samples of n-type doped TiO_2 (Nb1and NbF45, Fig. 6 Panels B and C respectively). In these two cases the spectral background (lines a) is not, of course, a flat line in that the n-type doped starting material contains a certain initial concentration of Ti^{3+}(I) species (see Fig. 3). The effect of irradiation in H_2 is surprising (lines b in Panels B and C) since an increase of the amount of Ti^{3+} species is, as expected, observed, however this is due uniquely to Ti^{3+}(I) whose intensity increases several times (but less than one order of magnitude) depending on the type of sample. No trace of species Ti^{3+}(II) is observed in the specific magnetic field region. In other words the presence of Ti^{3+} in the starting n-type doped materials seems selectively conditioning the fate of extra electrons injected in the solid, which all reach lattice Ti^{4+} sites preventing the formation of surface reduced centres. The intensities of the spectra after electron injection (hence the amount of reduced Ti^{3+} centres) is similar for the two doped samples (Fig. 6B and 6C) and slightly higher than that of the non-doped one (Fig. 6A).

3.5.2.Reduction of the solids by thermal annealing.

Titanium dioxide is a reducible oxide whose composition depends on the pressure of oxygen in the atmosphere. In particular, molecular oxygen is released upon annealing the solid under vacuum leaving excess electrons in the (reduced) solid[63]. This phenomenon, which has been deeply investigated by various techniques including EPR[20,64], can be represented as follows: $O^{2-} + 2Ti^{4+} \rightarrow$ ½ O_2 +$V_O^{\bullet\bullet}$+ $2Ti^{4+}$ +$2e^- \rightarrow$½ O_2 +$V_O^{\bullet\bullet}$+ $2Ti^{3+}$, where $V_O^{\bullet\bullet}$ indicates an empty oxygen vacancy according to the Kröger-Vink notation. Figure 7 compares the effects of a progressive reduction by annealing from rather mild conditions (373K under vacuum) till 773 K on the EPR spectra of bare (Panel A) and n-type doped (Panels B and C) anatase. The figure clearly shows that in the early stages of the reduction (lines b in the three Panels), Ti^{3+}(I) is the unique species formed in all materials indicating that the first fraction of excess electrons is stabilized on regular sites of the lattice. In the following stages of the treatment, the signal intensity of Ti^{3+} increases but the behaviour of the two classes of materials diverges. In the case of bare anatase (as documented in previous work[20]) the broad and featureless signal of Ti^{3+}(II) species (see Fig 3A) becomes soon dominant reflecting the complex situation based on reduced titanium centres in various coordination states, at the surface and subsurface regions. This complexity is increased, with respect to the case of simple electron injection (Fig.6) by the oxygen vacancies formed during the annealing. In the case of the n-type systems (F-TiO_2 or Nb-TiO_2, Fig. 7, Panels B-C), exactly as in the case of Fig. 6, it is indeed the signal of Ti^{3+}(I) which increases its intensity with increasing the solid reduction. At the same time the signals become broader and broader, though maintaining the axial structure (Panels B and C, lines b-e) because of dipolar interactions between similar centres in close vicinity due to their high concentration. In this case (Fig. 7) the intensity increment, much higher than in the case of electron injection (Fig. 6), is between one and two orders of magnitude according to the sample. At the highest annealing temperature the signal of F-TiO_2 (Panel B, line f) becomes featureless probably because the solid loses its n-type character due to the fluorine depletion (see Section 3.1). In the same conditions the niobium doped sample (Panel C) maintains its axial structure.

The described experiment confirms what was observed in the case of electron injection, i.e. the capability of the n-type doped materials to dilute extra electrons on the titanium sites of the oxide bulk producing high amounts of a single family of bulk reduced centres (Ti^{3+}(I)). This behaviour is different from that of bare TiO_2 for which, beside a small amount of Ti^{3+}(I), the much more abundant Ti^{3+}(II) centres are observed.

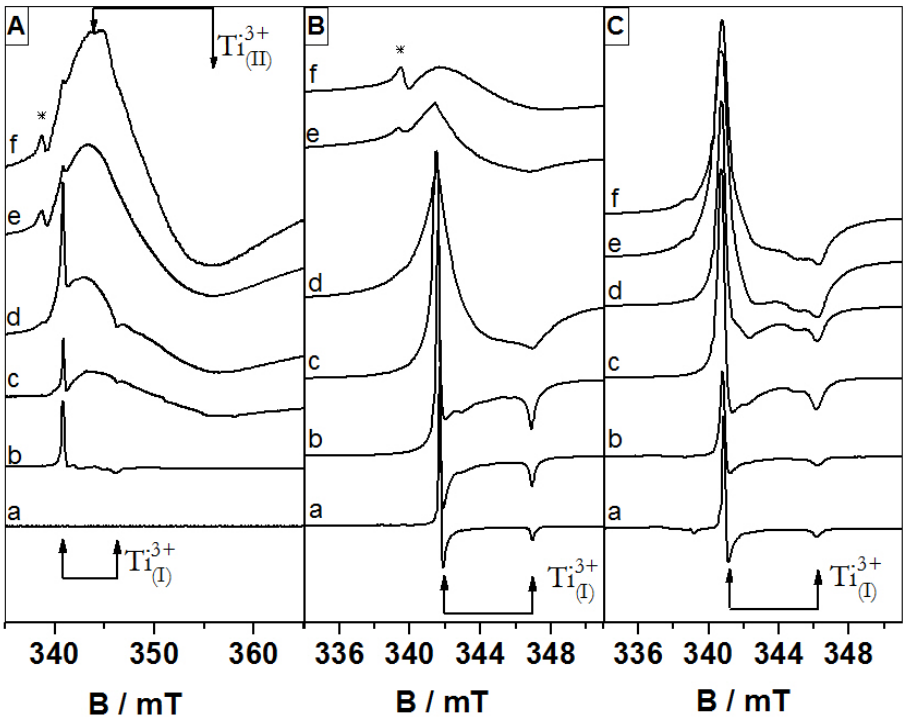

Figure 7. X-band CW-EPR spectra of: A) TiO_2, B) F2, and C) Nb1 samples subjected to annealing under vacuum at increasing temperature, recorded at 77 K . a) Fully oxidized starting materials; Annealing for 45 min at the following temperatures: b) 370 K, c) 470 K, d) 570 K, e) 670K, f) 770K. Notice the different magnetic field scale of panel A with respect to B and C. The star (*) indicates a signal (g = 2.003) ubiquitously present in reduced TiO_2.

In quantitative terms the amount of reduced centres in the two doped samples at the end of the reduction (Fig. 7Bf and 7Cf) is similar and one order of magnitude higher than that observed for the same samples after electron injection (Fig. 6). Also in this case the bare TiO_2 materials (7A) results less reducible than the doped ones (7 B,C).

3.5.3. Ti^{3+} centres obtained by thermal annealing in variously doped TiO_2 systems.

The results illustrated in the previous sections indicate that the n-type TiO_2 systems obtained by aliovalent excess electron doping show a different behaviour in electron trapping with respect to bare anatase. In order to understand whether this phenomenon is related to the presence of a generic heteroatom in the TiO_2 matrix, Ti^{3+} generation experiment by thermal annealing were carried out also on other doped systems with no n-type character. They were: zirconium doped TiO_2 (Zr-TiO_2) where Zr^{4+} substitutes Ti^{4+}cations (isovalent substitution[65]) and aluminium doped TiO_2 (Al-TiO_2). In this second case an aliovalent substitution occurs, with formation of a defective system (oxygen

vacancies compensate the lack of positive charge[66,67]). Both materials were prepared using the same procedure described in Section 2.

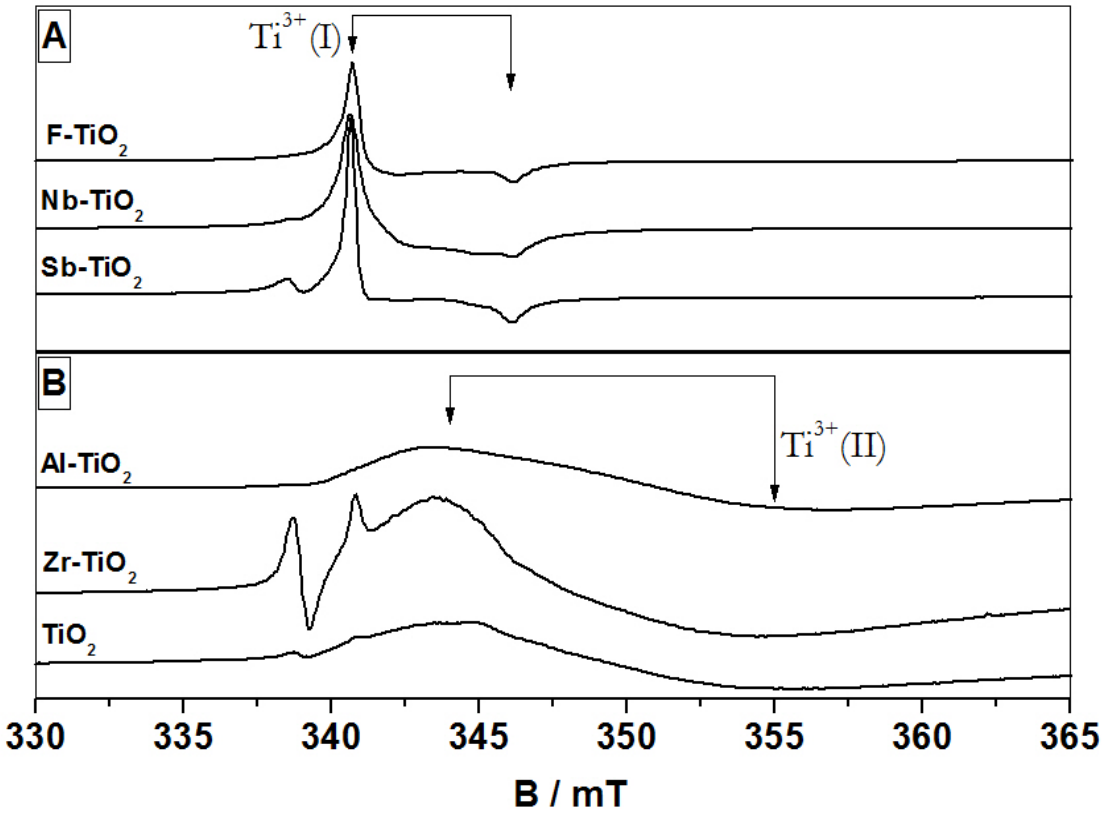

Figure 8. X-band CW-EPR spectra recorded at 77 K of variously doped titania samples annealed under vacuum at 770 K for 60 minutes.

In Fig. 8 the EPR spectra of n-type systems, including a sample not shown before (Sb-doped TiO_2) are compared with the spectra of the other sample of dopedTiO_2 after annealing in *vacuo* at 773 K. While all n-type doped materials (Fig. 8, Panel A) confirm the exclusive presence of Ti^{3+}(I) electron trapping centres (anatase bulk sites) after reduction, the two differently doped samples show the same behaviour of pristine anatase with the trapped electrons centres mainly confined to the disordered surface region (Ti^{3+}(II)).

The effect here discussed is therefore specific of n-type doped TiO_2 anatase (irrespective of the cationic or anionic nature of the aliovalent dopant) and it is not related to the presence of a generic heteroatom in the crystal lattice.

3.6. Optical properties of reduced materials.

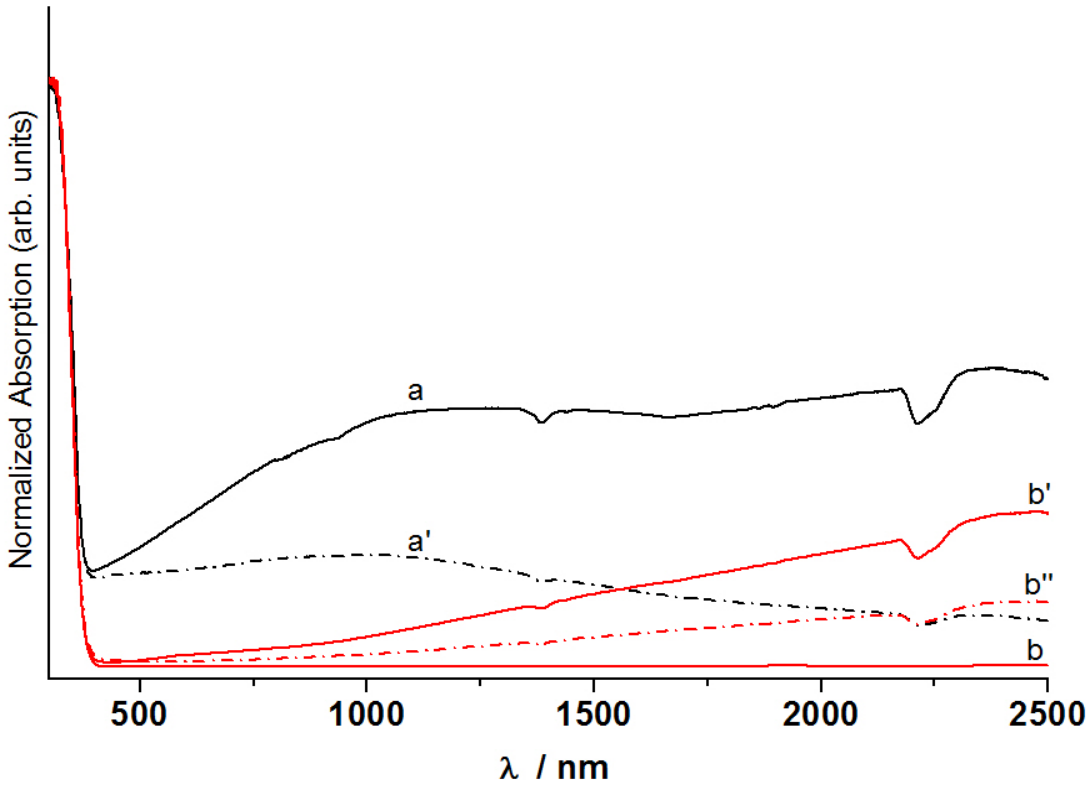

Figure 9. DR UV-Vis-NIR spectra of samples reduced upon thermal annealing under vacuum: a) pristine TiO_2 annealed at 770 K for 2h, a′) annealed TiO_2(a) after contact with O_2 at room temperature, b) fully oxidized, as prepared NbF25a, b′) NbF25a annealed under vacuum at 770K for 2 h, b″) annealed NbF25a (b') after contact with O_2 at room temperature.

In Fig. 9 the DR-UV-Vis-NIR spectra of TiO_2 and NbF25a samples reduced by annealing under vacuum at 770 K are reported.The annealing deeply modifies the optical properties of both pristine TiO_2 and n-type TiO_2. For these two kinds of materials in their fully oxidized state, in fact, no absorption from the band gap transition to 2500 nm is observed (Fig 9b for NbF25a). Upon annealing an onset of visible and NIR absorption occurs in parallel with the appearance of a blue color. In all the curves reported in Fig. 9, apart from minor absorption peaks at about 1400nm and 2250nm due to hydroxyl groups, the main spectral feature is represented by broad absorptions spread over the visible and infrared region. The spectra in Fig. 9 are confidently comparable one

with each other as the scattering properties should be similar for all samples which exhibit (Table 1) a similar crystallite size. Some trends in the Kubelka Munk Function may in fact be due to Rayleigh scattering rather than to optical absorption.

Broad optical spectra for reduced TiO_2 are reported in the literature, in particular in the case of rutile[68], which are attributed to the presence of Ti^{3+} centres responsible for the typical blue colour of these reduced systems. Once again, however, the n-type systems analysed in this work show a remarkable difference with respect to the pure material.

The reduced pure TiO_2 (Fig. 9a) shows a curve likely due to the superimposition of two broad absorptions, the former having a maximum around 1000nm (1.2 eV) and the second one at lower energy roughly corresponding to the instrumental threshold of 2500 nm (≤ 0.5 eV). The presence of the first absorption feature centred at c.a. 1000 nm is in agreement with data reported in the literature[68,69] and becomes much more evident after contacting the sample with oxygen at room temperature (Fig. 9a'). In these conditions, in fact, the fraction of the reduced centres absorbing at low energy preferentially reacts and the absorption curve centred at 1000 nm dominates the absorption spectrum after oxidation. The curves of the reduced n-type TiO_2 systems, unlike bare TiO_2, show a continuously increasing absorption with a maximum at very low energy (E ≤ 0.5 eV) again located near the instrumental threshold or even beyond 2500 nm (Fig. 9b′). The curve, in fact, is similar to those recently reported[26] for similar Nb-doped anatase systems with maximum at about 2500nm. Contacting the reduced n-type system with oxygen at RT (Fig. 9b″), as in the case of pure TiO_2, a fraction of the initial Ti^{3+} centres react but in this case only the overall intensity of the spectrum is affected and the absorption curve maintains its shape suggesting the presence of one absorption band only in this kind of system.

Furthermore, in order to characterize the Ti^{3+}centres in the n-type TiO_2 sample prepared in this work, valence band spectra were recorded after sample reduction by thermal annealing. In all cases it resulted impossible to observe Ti^{3+}centres in spite of the fact that the powders color turned from white to blue, the typical colour of reduced TiO_2[60,70]. This experimental evidence suggests that excess electrons rapidly migrate into the bulk of the material to form Ti^{3+}centres, in agreement with the conclusion drawn from EPR experiments.

4. Discussion and Conclusions.

The systems studied in this work, both singly doped or Nb-F co-doped materials, are n-type TiO_2. They contain in fact Nb and/or F, both carriers of an extra electron with respect to the elements of the stoichiometric oxide and, consequently, they all show the presence of $Nb^{5+}$and F^- (XPS) and of

Ti^{3+} ions (EPR). This latter fact, in particular, indicates that at least a fraction of the excess electrons introduced by the dopant is stabilized by valence induction as accounted for by the general formulas reported in section 3.3. An alternative possibility for the extra charge stabilization, which has been proposed in some case for Nb doped titania[24] is based on the formation of cationic vacancies (four Nb ions correspond to one Ti vacancy). It is not possible, on the basis of our data, to confirm or exclude the presence of such vacancies (which, by the way, are not easily detectable by experimental techniques). It must be kept in mind, however, that in general the aliovalently doped systems selectively choose the solution of higher stability and, therefore, the presence of Ti^{3+} ions seems to indicate the preference for the mechanism of valence induction rather than for that of vacancy formation.

The value of the energy band gap in n-type doped materials is a very complex problem. In all cases of co-doped samples we observed a small red shift of the edge of the band, in analogy to other published results[37,38,39,40,41] while in several other cases of Nb doping a blue shift is observed which is attributed to the Burstein-Moss effect. Our data (red shift for all F containing samples, lack of shift for the Nb-TiO_2 one) together with the variability of the results available in the literature suggest that the band gap value is dictated by a delicate interplay between the Burstein-Moss effect, the modifications occurring at the edge of the conduction band due to the presence of the energy levels of Ti^{3+} (vide infra) and those in the valence band causing the moving onwards of the band itself (see Section 3.4) .

The Ti^{3+}(I) centres observed by EPR at 77K determine the behaviour of the doped oxide. Previous work by our group has shown unambiguously that the reduced ions responsible of the EPR signal with $g_{\perp}$=1.992 and $g_{//}$=1.962 are placed in the regular lattice positions of the oxide bulk, i.e. they are not surface nor interstitial ions[20,44]. The energy levels corresponding to these excess electron centers are however extremely shallow or even lie at the edge the CB. This is indicated by the lack of absorption of the fully oxidized samples in the visible region and by the position of the Fermi level (Table 2) which is very high in the band gap or even lies in the conduction band. The correspondence between the structured and relatively narrow EPR signal (Fig. 4) of Ti^{3+}(I) and electronic centers located at the edge of the conduction band may seem paradoxical. However the nature of these centers is more complex than what apparently suggested by their simple X-band EPR spectrum. A previous investigation on the Ti^{3+}(I) centre performed by some of us using an oxide enriched in ^{17}O, has indeed shown that the spin density on the six oxygen ions surrounding Ti^{3+} is much lower than that found for systems in which the excess electron is localized in a d orbital of the titanium ion[20]. A comparison with the cases of the hexaaquo titanium(III)[71] and

with that of Ti^{3+} in interstitial sites of rutile[60] (both having a highly localized 3d electron) showed unequivocally the particular nature of Ti^{3+}(I) in anatase whose electron seems to be delocalized beyond the first coordination sphere. Moreover, top level DFT calculations recently published by Pacchioni and coworkers [17] have found that there are two possible solutions for lattice Ti^{3+} centers in F or Nb doped TiO_2 having the same total energy. The first one describes a fully localized system while the second shows the electron density delocalized on all the metal ions of the supercell, the energy of these states being at the bottom of the conduction band[17]. If theoretical calculations does not allow a choice between these two solutions, the data related to the oxygen spin density and those here reported (position of the Fermi level), clearly point to a delocalized model. The excess electron centers detected by EPR, Fig 3, are thus responsible of the conduction of the solid which has been measured for Nb-TiO_2 materials and resulted to be higher than that of pure titania[24]. The fact that no optical absorption is observed for the as prepared samples despite the presence of Ti^{3+} centers (Fig. 9, b') is likely due to the relatively low initial concentration of these centers and to their extremely broad absorption features.

As shown by the recent paper of Di Trizio *et al.*[26] n-type doped anatase can be prepared and used in reduced state. We have here shown that the presence of excess electrons centers seriously affects the processes of reduction of the n-type doped systems producing solids markedly differing from reduced anatase. As clearly shown by Figure 7 the annealing and the simultaneous depletion of oxygen implies the formation of the same type of bulk reduced centers already present in the starting material (Ti^{3+}(I)) which assume an homogeneous distribution into the bulk. The conduction properties of the starting n-type material[24,25] are likely responsible for conveyng the excess electrons formed upon reduction to form this homogeneous distribution of reduced.This is not the case of pristine anatase for which the great majority of reduced centers correspond to the EPR signal of Ti^{3+}(II) that is to centers present at the surface or subsurface of the nanoparticles in a highly heterogeneous environment because of both the surface morphology and the presence of the oxygen vacancies formed upon annealing. This description is supported by both photoelectron spectroscopy and optical spectra (Fig.9). XPS is a surface sensitive technique and does not detect Ti^{3+} species in the starting doped materials (Fig.4) and even after reduction. The optical spectra basically indicate two facts: a) the doped systems absorb visible and NIR light when reduced; b) similarly to the case of EPR spectra, the optical absorptions obtained reducing pristine and n-type doped anatase, are different. In particular, in the early stages of reduction pure anatase mainly absorbs in two regions of the spectrum (maxima at 1000 nm and 2500 nm) while in the case of n-type doped materials the second type of absorption only is present (Fig.9). This agrees with the

EPR results indicating that the reduced n-type materials are simpler (only one EPR signal) and more homogeneous than the reduced TiO_2. Furthermore the optical spectra firmly indicate that the reduced states of n-type TiO_2 are shallower than the majority of those present in reduced pure anatase. This is in agreement with the position of the Fermi level (Table 2) derived combining the UPS and optical spectra. The simplified physical states of the two types of materials in their stoichiometric and reduced states are schematically compared in the following (Scheme 1) on the basis of the findings reported in this paper.

In conclusion, concerning the description of n-type doped anatase, this work has served to put some important pieces of the patchwork into place and we can now look at this system as a solid markedly different from pure anatase. In fact n-type doped anatase contains very shallow donor levels whose amount increases upon reduction because the solid is able to homogeneously scatter the excess electrons by associating them with regular titanium ions of the lattice (Ti^{3+}(I)). The same does not occur for pure anatase which, when reduced, preferentially forms deeper (Ti^{3+}(II)) centers localized at surface and subsurface sites. The particular position of Ti^{3+}(I) at the lower limit of the conduction band also explains conductivity measurements placing Nb-F doped materials at the boundary between a true n-doped semiconductor and a metallic conductor[53,54,55] and accounts for recent results indicating the delocalized nature of the wave function of the Ti^{3+}(I) unpaired electron.

All these features are of fundamental importance in the field of Transparent Conducting Oxides (TCO) and have a further appealing consequence related to the solid reduction in a homogeneous way, with creation of absorption in the visible and in the NIR (Fig.8) without producing an accumulation of electrons at surface. This could have much interest in view of the preparation of reduced titania based photocatalytic systems capable of absorbing visible and NIR radiation as recently proposedby several Authors[72,73,74].

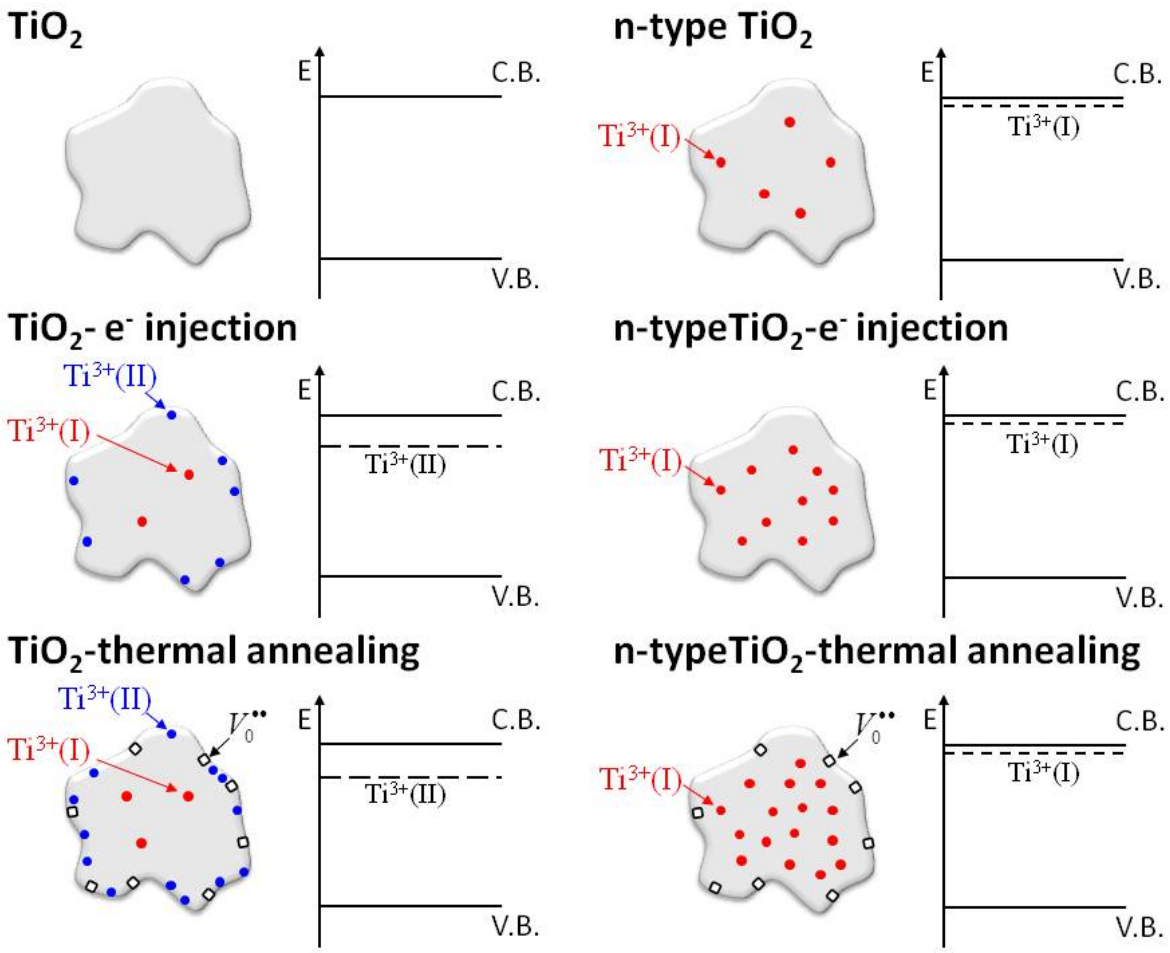

Scheme 1.

Acknowledgements

This work has been supported by the Italian Ministry of University and Research, MIUR, through the "Programs of National Relevance" (PRIN-2009) and the "National Funding for Basic Research" (FIRB) with a project entitled "Oxides at the nanoscale: functionalities and applications" (FIRB RBAP11AYN). Thanks are also due to the COST Action CM1104 (Reducible oxides: chemistry, structure and functions). The μ-XRFresults have been obtained with the equipment acquired by the "G. Scansetti" Interdepartmental Centre for Studies on Asbestos and Other Toxic Particulates, thanks to a grant by the Compagnia di San Paolo, Torino, Italy.

TOC

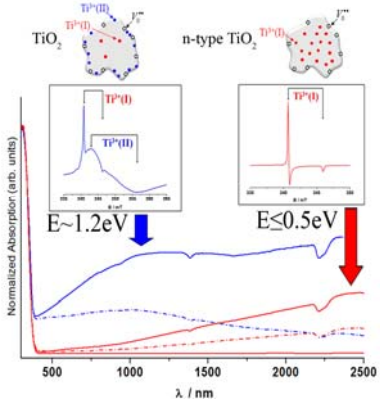

References

[1]Thompson, T. L.; Yates Jr., J. T. Surface Science Studies of the Photoactivation of TiO_2-New Photochemical Processes. *Chem. Rev.* **2006**, *106*, 4428-4453

[2] Henderson, M. A. A Surface Science Perspective on TiO_2 Photocatalysis. *Surf. Sci. Reports* **2011**, *66*, 185-297.

[3] Serpone, N.; Pelizzetti, E. *Photocatalysis: Fundamentals and Applications*; Wiley & Sons, 1989.

[4] Fujishima, A.; Honda, K. Electrochemical Photolysis of Water at a Semiconductor Electrode. *Nature* **1972**, *238*, 37-38.

[5] Cho, M.; Chung, H.; Choi, W.; Yoon, J. Linear Correlation Between Inactivation of E. coli and OH Radical Concentration in TiO_2 Photocatalytic Disinfection. *Water Research* **2004**, *38*, 1069-1077.

[6] Nozawa, M.; Tanigawa, K.; Hosomi, M.; Chikusa, T.; Kawada, E. Removal and Decomposition of Malodorants by Using Titanium Dioxide Photocatalyst Supported on Fiber Activated Carbon. *Wat. Sci. Technol.* **2001**, *44*, 127-133.

7 Watanabe, T.; Nakajima, A.; Wang, R.; Minabe, M.; Koizumi, S.; Fujishima, A.; Hashimoto, K. Photocatalytic Activity and Photoinduced Hydrophilicity of Titanium Dioxide Coated Glass. *Thin Solid Films* **1999**, *351*, 260-263.

[8] Hagfeld, A.; Grätzel, M. Light-Induced Redox Reactions in Nanocrysyalline Systems. *Chem. Rev.* **1995**, *95*, 49-68.

[9] Asahi, R.; Morikawa, T.; Ohwaki, T.; Aoki, K.; Taga, Y. Visible Light Photocatalysis in Nitrogen-Doped Titanium oxides. *Science* **2001**, *293*, 269-271.

[10] Fujishima, A.; Zhang, X.; Tryk, D. A. TiO_2 and Related Surface Phenomena. *Surf. Sci. Reports* **2008**, *63*, 515-582.

[11] Di Valentin, C.; Finazzi, E.; Pacchioni, G.; Selloni, A.; Livraghi, S.; Paganini, M. C.; Giamello, E. N-Doped TiO_2: Theory and Experiment. *Chem. Phys.* **2007**, *339*, 44-56 .

[12] J Yu, J. C.; Yu, J.; Ho, W.; Jiang, Z.; Zhang, L. Effect of F^- Doping on the Photocatalytic Activity and Microstructure of Nanocrystalline TiO_2 Powders. *Chem. Mater.* **2002**, *14*, 3808-3816.

[13]Li, D.; Haneda, H.; Labhsetwar, N.; Hishita, S.; Ohashi, N. Visible-Light-Driven Photocatalysis of Fluorine-Doped TiO_2 Powders by Creation of Surface Oxygen Vacancies. *Chem. Phys. Lett.* **2005**, *401*, 579-584.

[14] Czoska, A.; Livraghi, S.; Chiesa, M.; Giamello, E.; Agnoli, S.; Granozzi, G.; Finazzi, E.; Di Valentin, C.; Pacchioni, G. The Nature of Defects in Flurine-Doped TiO_2. *J. Phys. Chem. C* **2008**, *112*, 8951-8956.

[15] Subbarao, S. N.; Yun, Y. H.; Kershaw, R.; Dwight, K.; Wold, A. Electrical and Optical Properties of the System $TiO_{2-x}F_x$. *Inorg. Chem.* **1979**, *18*, 488-492.

[16] Wang, C. M.; Mallouk, T. E. Photoelectrochemistry and Interfacial Energetics of Titanium Dioxide Photoelectrodes in Fluoride-Containing Solution. *J. Phys. Chem.* **1990**, *94*, 423-428.

[17] Di Valentin, C.; Pacchioni, G.; Selloni, A. Reduced and n-Type Doped TiO_2: Nature of Ti^{3+} Species. *J. Phys. Chem. C* **2009**, *113*, 20543-20552.

[18] Valigi, M.; Cordischi, D.; Minelli, G.; Natale, P.; Porta, P.; Keijzers, C. P. A Structural, Thermogravimetric, Magnetic, Electron Spin Resonance, and Optical Reflectance Study of the NbO_xTiO_2 System. *J. Solid State Chem.* **1988**, *77*, 255-263.

[19] Kiwi, J.; Suss, J. T.; Szapiro, S. EPR Spectra of Niobium-Doped TiO_2 and Implications for Water Photocleavage Processes. *Chem. Phys. Lett.* **1984**, *106*, 135-138.

[20] Livraghi, S.; Chiesa, M.; Paganini, M. C.; Giamello, E. On the Nature of Reduced States in Titanium Dioxide As Monitored by Electron Paramagnetic Resonance. I: The Anatase Case. *J. Phys. Chem. C* **2011**, *115*, 25413-25421.

[21] Furubayashi, Y.; Hitosugi, T.; Yamamoto, Y.; Inaba, K.; Kinoda, G.; Hirose, Y.; Shimada, T.; Hasegawa, T. A Transparent Metal Nb-Doped TiO_2. *Appl. Phys. Lett.* **2005**, *86*, 252101.

[22] Zhang, S. X.; Dhar, S.; Yu, W.; Xu, H.; Ogale, S. B.; Venkatesan, T. Growth Parameter-Property Phase Diagram for Pulsed Laser Deposited Transparent Oxide Conductor Anatase Nb:TiO_2. *App. Phys. Lett.* **2007**, *91*, 112113.

[23] Su, W.; Song, K.; Huo, D.; Li, B. Analysis of Correlation Between Electrical and Infrared Optical Properties of Anatase Nb Doped TiO_2 Films. *Curr. Appl. Phys.* **2013**, *13*, 556-561.

[24] Chandiran, A.; K. Sauvage, F.; Casas-Cabanas, M.; Comte, P.; Zakeeruddin, S. M.; Grätzel, M. Doping a TiO_2 Phoanode with Nb^{5+} to Enhance Transparency and Charge Collection Efficiency in Dye-Sensitized Solar Cells. *J. Phys. Chem. C* **2010**, *114*, 15849-15856.

Hopper, E. M.; Sauvage, F.; Chandiran, A.K.; Grätzel, M.; Poeppelmeier, K.R.; Mason, T.O. Electrical Properties of Nb-, Ga-, and Y-Substituted Nanocrystalline Anatase TiO_2 Prepared by Hydrothermal Synthesis. *J. Am. Chem. Soc.* **2012**, *95,* 3192-3196.

[26] De Trizio, L.; Buonsanti, R.; Schimpf, A. M.; Llordes, A.; Gamelin, D. R.; Simonutti, R.; Milliron, D. J. Nb-Doped Colloidal TiO_2 Nanocrystals with Tunable Infrared Absorption. *Chem. Mater.* **2013**, *25*, 3383-3390.

[27] P Chester, P. Cross-Doping Agent for Rutile Masers. *J. Appl. Phys.* **1961**, *32*, 866-868.

[28] Zimmermann, P. H. Temperature Dependence of the EPR Spectra of Niobium- Doped TiO_2. *Phys. Rev. B* **1973**, *8*, 3917-3927.

[29] Gao, Y.; Chambers S.A. MBE Growth and Characterization of Epitaxial TiO_2(110) Surface by Molecular Beam Epitaxy. *Mat. Lett.* **1996**, *26*, 217-221.

[30] Dozzi, M. V.; Livraghi, S.; Giamello, E.; Selli, E. Photocatalytic Activity of S- and F-Doped TiO_2 in Formic Acid Mineralization. *Photochem. Photobiol. Sci.* **2011**, *10*, 343-349.

[31]Material Analysis Using Diffraction, available at http://www.ing.unitn.it/~maud.

[32] Morris, D.; Dou, Y.; Rebane, J.; Mitchell, C.E.J.; Egdell, R.G.; Law, D.S.L.; Vittadini, A.; Casarin, M. Photoemission and STM Study of the Electronic Structure of Nb-Doped TiO_2. *Phys. Rev. B* **2000**, *61*, 13445-13457

[33]Di Paola, A.; Cufalo, G.; Addamo, M.; Bellardita, M.; Campostrini, R.; Ischia, M.; Ceccato, R.; Palmisano, L. Photocatalytic Activity of Nanocrystalline TiO_2 (Brookite, Rutile and Brookite-Based) Powders Prepared by Thermohydrolysis of $TiCl_4$ in Aqueous Chloride Solutions. *Colloids Surf. A* **2008**, *317*, 366-376.

[34] Kurita, D.; Ohta, S.; Sugiura, K.; Ohta, H.; Koumoto, K. Carrier Generation and Transport Properties of Heavily Nb-Doped Anatase TiO_2 Epitaxial Films at High Temperatures. *J. App. Phys.* **2006**, *100,* 096105.

[35] Zhang, S.X.; Kundaliya, D.C.; Yu, W.; Dhar, S.; Yung, S.Y.; Salamnca-Riba, L.G.; Ogale, S.B.; Vispute, R.D.; Venkatesan, T. Niobium doped TiO_2: Intrinsic Transparent Metallic Anatase Versus Highly Resistive Rutile Phase. *J. App. Phys.* **2007**, *102*, 013701.

[36]Breault, T. M.; Bartlett, B. M. Composition Dependence of TiO_2:(Nb,N)- x Compounds on the Rate of Photocatalytic Methylene Blue Dye Degradation. *J. Phys. Chem. C* **2013**, *117*, 8611-9618.

[37]Zakrzewska, K.; Radecka, M.; Rekas, M. Effect of Nb, Cr, Sn, Additions on Gas sensing properties of TiO_2 Thin Films. *Thin Solid Films* **1997**, *310*, 161-166.

[38]Mattsson, A.; Leideborg, M.; Larsson, K.; Westin, G.; Orsterlund, L. Absorption and Solar Light Decomposition of acetone on anatase TiO_2 and Niobium Doped TiO_2 Films. *J. Phys. Chem. B* **2006**, *110*, 1210-1220.

[39] Hirano, M.; Ichihashi, Y. Phase Transformation and Precipitation Behavior of Niobium Component Out of Niobium-Doped Anatase-Type TiO_2 Nanoparticles Synthesized Via Hydrothermal Crystallization. *J. Mater. Sci.* **2009**, *44*, 6135-6143.

[40]Kubacka, A.; Colon, G.; Fernandez-Garcıa, M. Cationic (V, Mo, Nb, W) Doping of TiO_2-Anatase: a Real Alternative for Visible Light-Driven Photocatalysis. *Catal. Today* **2009**, *143*, 286-292.

[41] Znad, H.; Ang, M. H.; Tade, M. O. Ta/TiO_2-and Nb/TiO_2-Mixed Oxide as Efficient Solar Photocatalytic: Preparation, Characterization, and Photocatalytic Activity. *Int. J. Photoenergy* **2012**, Article ID 548158.

[42]Tsvetkov, N. A.; Larina, L. L.; Shevaleevskiy, O.E.; Al-Ammar, A.B.; Ahn, T. Design of Conduction Band Structure of TiO_2 Electrode Using Nb Doping for Highly Efficient Dye-Sensitized Solar Cells. *Prog. Photovoltaics* **2012**, *20*, 904-911.

[43] Mardare, D.; Tasca, M.; Delibas, M.; Rusu, G. I. On the structural Properties and Optical Transmittance of TiO_2 r.f. Sputtered Thin Films. *Appl. Surf. Sci.* **2000**, *156*, 200-206.

[44] Chiesa, M.; Paganini, M. C.; Livraghi, S.; Giamello, E. Charge Trapping in TiO_2 Polymorphs As Seen by Electron Paramagnetic Resonance Spectroscopy. *Phys. Chem. Chem. Phys.* **2013**, *15*, 9435-9447.

[45] Sasahara, A.; Tomitori, M. XPS and STM Study of Nb-Doped TiO_2(110)-(1x1) Surface. *J. Phys. Chem. C*, **2013**, *117*, 17680-17686.

[46] Yeh, J.J.; Lindau, I. Atomic Subshell Photonization Cross Sections and Asymmetry Parameters: $1 \leq Z \leq 103$. *Atomic Data and Nuclear Data Tables* **1985**, *32*, 1-155.

[47] Tanuma, S.; Powell, C. J.; Penn, D. R. Calculations of electron Inelastic Mean Free Paths. *Surf. Interf. Anal.* **1994**, *21*, 165-176.

[48]Sandell, A.; Sanyal, B.; Walle, L.E.; Uvdal, P.; Borg, A. Probing the Conduction Band Edge of Transition Metal Oxides by X-Ray Absorption Spectroscopy. *J. Electron. Spectrosc.* **2011**, *183*, 107-113.

[49] Walle, L. E.; Agnoli, S.; Svenum, I.-H.; Borg, A.; Artiglia, L.; Krger, P.; Sandell, A.; Granozzi, G. High Resolution Photoemission and X-Ray Absorption Spectroscopy of a Lepidocrocite-like TiO_2 Nanosheet on Pt(110) (12). *J. Chem. Phys.* **2011**, *135*, 054706.

[50] Nikolay, T.; Larina, L.; Shevaleevskiy, O.; Ahn, B. T. Electronic Structure Study of Lightly Nb-Doped TiO_2 Electrode for Dye-Sensitazied Soalr Calls. *Energy Environ. Sci.* **2011**, *4*, 1480-1486.

[51] Martra, G; Gianotti, E.; Coluccia, S.; *The application of UV-Visible-NIR Spectroscopy to Oxides.* Chapter two in Hargraves, J.S.J.; Jackson, D.; *Metal Oxide Catalysis* Wiley-VCH, 2008.

[52] Chambers, S.A.; Liang, Y.; Yu, Z.; Droopad, R.; Ramandi, J.; Eisenbeiser, K. Band Discontinuities at Epitaxial $SrTiO_3$/Si(001) Heterojunctions. *Appl. Phys. Lett.* **2000**, *77*, 1662-1664.

[53] Archana, P.S.; Jose, R.; Yosoff, M.M.; Ramakrishna, S. Near Band-Edge Electron in Electrospun Nb-doped Anatase Nanofibers Probed by Electrochemical Impedence Spectroscopy Appl. Phys. Lett. 2011, 98, 152106.

[54] Hitosugi, T.; Kamisaka, H.; Yamashita, K.; Nogawa, H.; Furubayashi, Y.; Nakao, S.; Chikamatsu, A.; Kumigashira, H.; Oshima, M.; Hirose, Y.; Shimada, T.; Hasegawa. T. Electronic Band Structure of Transparent Conductor: Nb-Doped Anatase TiO_2. *Appl. Phys. Express* **2008**, *1*, 111203.

[55] Liu, X.D.; Jiang, E.Y.; Li, Z.Q.; Song, Q.G. Electronic Structure and Optical Properties of Nb-Doped Anatase TiO_2 Appl. Phys. Lett. 2008, 92, 252104

[56] Deskins N. A.; Dupuis, M. Intrinsic Hole Migration Rates in TiO_2 from Density Functional Theory. *J. Phys. Chem. C* **2009**, *113*, 346-358.

[57] Deskins, N. A. ; Rousseau R.; Dupuis, M. Defining the Role of Excess Electrons in the Chemistry of TiO_2. *J. Phys. Chem. C* **2010**, *114*, 5891-5897.

[58] Krüger, P.; Bourgeois, S.; Domenichini, B.; Magnan, H.; Chandesris, D.; Le Fevre, P.; Flank, A. M.; Jupille, J.; Floreano, L.; Cossaro, A.; Verdini A.; Morgante, A. Defect States in the TiO_2(110) Surface Probed by Resonant Photoelectron Diffraction. *Phys. Rev. Lett.* **2008**, *100*, 055501.

[59] Wendt, S.; Sprunger, P. T.; Lira, E.; Madsen, G. K. H. M.; Li, Z. Hansen, J.; Matthiensen,J.; Blekinge-Rasmussen, A.; Lægsgaard, E.; Hammer B.; Besenbacher, F. The Role of Interstitial Sites in the Ti3d Defects State in the Band Gap of Titania. *Science*, **2008**, *320*, 1755-1759.

[60] Livraghi, S.; Maurelli, S.; Paganini, M.C.; Chiesa, M.; Giamello, E. Probing the Local Environment of Ti^{3+} Ions in TiO_2 (Rutile) by ^{17}O HYSCORE. *Angew. Chem. Intern. Ed.* **2011**, *50*, 8038-8040.

[61] Chiesa, M.; Paganini, M.C.; Giamello, E.; Murphy, D. M.; Di Valentin, C.; Pacchioni, G. Excess Electrons Stabilization on Ionic Oxide Surfaces. *Acc. Chem. Res.* **2006**, *39*, 861-867.

[62] Berger, T.; Diwald, O.; Knoezinger, E.; Napoli, F.; Chiesa M.; Giamello, E. Hydrogen Activation at TiO_2 Anatase Nanoparticles. *Chem. Phys.* **2007**, *339*, 138-145.

[63] Diebold, U. The Surface Science of Titanium Dioxide. *Surf. Sci. Reports* **2003**, *48*, 53-229.

[64] Carter, E.; Carley, A. F.; Murphy, D. M. Evidence for O_2^- Radical Stabilization at Surface Oxygen Vacancies on Polycrystalline TiO_2. *J. Phys. Chem. C* **2007**, *111*, 10630-10638.

[65] Livraghi, S.; Olivero, F.; Paganini, M. C.; Giamello E. Titanium Ions Dispersed into the ZrO_2 Matrix: Spectroscopic Properties and Photoinduced Electron Transfer *J. Phys. Chem. C* **2010**, *114,* 18553-18558.

[66] Shirley, R.; Kraft, M.; Inderwildi O. R. Electronic and Optical Properties of Aluminium-Doped Anatase and Rutile TiO_2 From Ab Initio Calculation. *Phys. Rev. B: Cond. Mat. Mat. Phys*. **2010**, *81*, 075111.

[67] M Steveson, M.; Bredow, T. A.; Gerson R. MSINDO Quantum chemical Modelling Study of the Structure of Aluminium-doped TiO_2. *Phys. Chem. Chem. Phys*. **2002**, *4*, 358-365.

[68] Khomenko, V.M.; Langer, K.; Rager, H.; Fett, A. Electronic Absorption by Ti^{3+} Ions and Electron Delocalization in Synthetic Blue Rutile. *Phys. Chem. Minerals* **1998**, *25,* 338-346.

[69] Komaguchi, K.; Maruoka, T.; Nakano, H.; Imae, I.; Ooyama, Y.; Harima, Y. Electron-Transfer Reaction of Oxygen Species on TiO_2 Nanoparticles Induced by Sub-Band-Gap Illumination. *J. Phys. Chem. C* **2010**, *114*, 1240-1245.

[70] Diebold, U.; Li, M.; Dulub, O.; Hebenstreit, E.L.D.; Hebenstreit, W. The Relationship Between Bulk and Surface Properties of Rutile TiO_2(110). *Surf. Rev. Lett.* **2000**, *5-6*, 613-617.

[71] Maurelli, S.; Livraghi, S.; Chiesa, M.; Giamello, E.; Van Doorslaer, S.; Di Valentin, C.; Pacchioni, G. Hydration Structure of the Ti(III) Cation as Revealed by Pulse EPR and DFT Studies: New Insights into a Textbook Case. *Inorg. Chem.* **2011**, *50*, 2385-2394.

[72] Zuo, F.; Wang, L.; Wu, T.; Zhang, Z.; Borchardt, D.; Feng, P. Self-Doped Ti^{3+} Enhanced Photocatalyst for Hydrogen Production Under Visible Light. *J. Am. Chem. Soc.* **2010**, *132*, 11856-11857.

[73] Gordon, T. R.; Cargnello, M.; Paik, T.; Mangolini, F.; Weber, R. T.; Fornasiero, P.; Murray, C. B. Nonaqueous synthesis of TiO_2 Nanocrystals Using TiF_4 to Engineer Morphology, Oxygen Vacancy Concentration, and Photocatalytic Activity. *J. Am. Chem. Soc.* **2012**, *134*, 6751-6761.

[74] Grabstanowicz, L. R.; Gao, S.; Li, T.; Rickard, R. M.; Rajh, T.; Liu, D-J.; Xu, T. *Inorg. Chem.* Facile Oxidative Conversion of TiH_2 to High-Concentration Ti^{3+}-Self-Doped-TiO_2 with Visible Light Photoactivity. **2013**, *52*, 3884-3890.